Article

Role of Surface Dimer Dynamics in Creating Ordered Organic–Semiconductor Interfaces

Robin L. Hayes, and Mark E. Tuckerman

J. Am. Chem. Soc., **2007**, 129 (40), 12172-12180• DOI: 10.1021/ja0724994 • Publication Date (Web): 19 September 2007

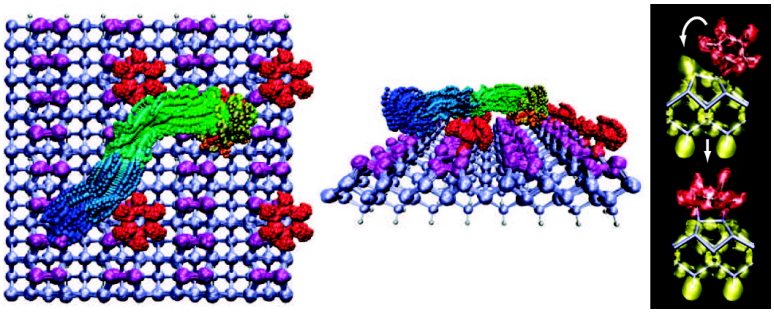

More About This Article

Additional resources and features associated with this article are available within the HTML version:

- Supporting Information
- Access to high resolution figures
- Links to articles and content related to this article
- Copyright permission to reproduce figures and/or text from this article

View the Full Text HTML

J|A|C|S
ARTICLES
Published on Web 09/19/2007

Role of Surface Dimer Dynamics in Creating Ordered Organic−Semiconductor Interfaces

Robin L. Hayes[†] and Mark E. Tuckerman*[,†,‡]

Contribution from the Department of Chemistry, and Courant Institute of Mathematical Sciences, New York University, New York, New York 10003

Received April 10, 2007; E-mail: mark.tuckerman@nyu.edu

Abstract: Understanding the chemical reaction mechanisms governing how small organic molecules attach to semiconductor surfaces can lead to new strategies for creating specific surface patterns such as single adduct monolayers. In this study, room-temperature ab initio molecular dynamics simulations of one and two 1,3-cyclohexadiene (CHD) molecule(s) reacting with the Si(100)-2×1 surface reveal that adducts form via a carbocation-mediated two-step mechanism. Dimer flipping can either promote or prevent bond formation depending on how the CHD approaches. CHDs often travel past several Si dimers before finding the proper local environment. The resulting intermediate can persist for more than 4 ps, allowing the second bond to form with any adjacent Si dimer. The additional reactive site accounts for a large portion of the discrepancy between the predicted thermodynamic and observed experimental product distribution. Surface adducts protect a 5.6 Å region, direct unbound CHD exploration, and can cause adjacent dimers to flip.

1. Introduction

The design of well-ordered, self-assembled organic nanostructures on semiconducting surfaces promises to combine the rich functionality of organic and biological systems with the well-established semiconducting infrastructure.[1−14] The long-term vision includes lithography with atomic resolution, sensors for specific toxins or pollutants, and molecular computing. The underlying assumption is that controllable organic−inorganic interfaces are feasible. Indeed, there has been some success in obtaining locally ordered structures on the hydrogen terminated Si(100) surface.[15−19] These methods require a dangling Si bond without a H to initialize the self-replicating reaction. In contrast, another popular approach eliminates the initialization step by exploiting the reactivity between surface dimers, which form on the bare (100) surface of Si, Ge, and SiC, with π-bonds in organic molecules. Charge asymmetry on Si, arising from dimer tilting, allows the violation of Woodward−Hoffmann selection rules, resulting in a variety of possible [2+2] and [4+2] surface adducts.[10] Which adduct forms depends on the orientation between the dimer and the π-system. For the most part, multiple surface adducts create disordered nanostructures ill-suited to nanotechnology applications.

Cycloaddition of 1,3-cyclohexadiene (CHD) with the Si(100)-2×1 surface exemplifies the challenges inherent in further developing this technology. STM experiments[20−23] have identified at least five distinct adducts, displaying the bonding flexibility of these types of systems. Theoretical studies, in the form of static cluster calculations[24−26] and density functional theory (DFT) periodic calculations,[27,28] have identified stable structures and suggested possible reaction mechanisms. However, the predicted product distribution based solely on thermodynamics is at odds with what is observed experimentally. Minary and Tuckerman used Car−Parrinello driven ab initio molecular dynamics (AIMD)[29] and obtained a product distribution for the closely related 1,3-butadiene system consistent with

[†] Department of Chemistry.
[‡] Courant Institute of Mathematical Sciences.

(1) Faber, E.; Sparreboom, W.; Groeneveld, W.; de Smet, L.; Bomer, J.; Olthuis, W.; Zuilhof, H.; Sudholter, E.; Bergveld, P.; van den Berg, A. *ChemPhysChem* **2007**, *8*, 101−112.
(2) He, J.; Chen, B.; Flatt, A.; Stephenson, J.; Condell, D.; Tour, J. *Nat. Mater.* **2006**, *5*, 63−68.
(3) Cattaruzza, F.; Cricenti, A.; Flamini, A.; Girasole, M.; Longo, G.; Prosperi, T.; Andreano, G.; Cellai, L.; Chirivino, E. *Nucleic Acids Res.* **2006**, *34*, e32.
(4) Wei, F.; Qu, P.; Zhai, L.; Chen, C.; Wang, H.; Zhao, X. *Langmuir* **2006**, *22*, 6280−6285.
(5) Pitters, J.; Wolkow, R. *Nano Lett.* **2006**, *6*, 390−397.
(6) Guisinger, N.; Greene, M.; Basu, R.; Baluch, A.; Hersam, M. *Nano Lett.* **2004**, *4*, 55−59.
(7) Lu, W.; Meunier, V.; Bernholc, J. *Phys. Rev. Lett.* **2005**, *95*, 206805.
(8) Cai, W.; Peck, J.; van der Weide, D.; Hamers, R. *Biosens. Bioelectron.* **2004**, *19*, 1013−1019.
(9) Rakshit, T.; Liang, G.; Ghosh, A.; Datta, S. *Nano Lett.* **2004**, *4*, 1803−1807.
(10) Filler, M.; Bent, S. *Prog. Surf. Sci.* **2003**, *73*, 1−56.
(11) Bent, S. *Surf. Sci.* **2002**, *500*, 879−903.
(12) Lu, X.; Lin, M. *Int. Rev. Phys. Chem.* **2002**, *21*, 137−184.
(13) Kruse, P.; Wolkow, R. *Appl. Phys. Lett.* **2002**, *23*, 4422−4424.
(14) Wolkow, R. *Annu. Rev. Phys. Chem.* **1999**, *50*, 413−441.
(15) Basu, R.; Kinser, C.; Tovar, J.; Hersam, M. *Chem. Phys.* **2006**, *326*, 144−150.
(16) Pitters, J.; Dogel, I.; DiLabio, G.; Wolkow, R. *J. Phys. Chem. B* **2006**, *110*, 2159−2163.
(17) Hossain, M.; Kato, H.; Kawai, M. *J. Am. Chem. Soc.* **2005**, *127*, 15030−15031.
(18) Kirczenow, G.; Piva, P.; Wolkow, R. *Phys. Rev. B* **2005**, *72*, 245306.
(19) Lopinski, G.; Wayner, D.; Wolkow, R. *Nature* **2000**, *406*, 48−51.
(20) Teague, L.; Boland, J. *Thin Solid Films* **2004**, *464−465*, 1−4.
(21) Teague, L.; Boland, J. *J. Phys. Chem. B* **2003**, *107*, 3820−3823.
(22) Kong, M.; Teplyakov, A.; Jagmohan, J.; Lyubovitsky, J.; Mui, C.; Bent, S. *J. Phys. Chem. B* **2000**, *104*, 3000−30007.
(23) Hovis, J.; Liu, J.; Hamers, R. *J. Phys. Chem. B* **1998**, *102*, 6873−6879.
(24) Lee, H.; Choi, C.; Gordon, M. *J. Am. Chem. Soc.* **2005**, *127*, 8485−8491.
(25) Choi, C.; Gordon, M. *J. Am. Chem. Soc.* **1999**, *121*, 11311−11317.
(26) Konecny, R.; Doren, D. *J. Am. Chem. Soc.* **1997**, *119*, 11098−11099.
(27) Fan, X.; Zhang, Y.; Lau, W.; Liu, Z. *Phys. Rev. B* **2005**, *72*, 165305.
(28) Teague, L.; Chen, D.; Boland, J. *J. Phys. Chem. B* **2004**, *108*, 7827−7830.
(29) Car, R.; Parrinello, M. *Phys. Rev. Lett.* **1985**, *55*, 2471−2474.

10.1021/ja0724994 CCC: $37.00

the experimental product distribution of 1,3-cyclohexadiene.[30,31] Given the variety of bonding motifs and the apparent kinetic effects, 1,3-CHD on Si(100)-2×1 provides an ideal test case to examine the role played by surface dynamics in adduct formation.

Our primary goal is to understand how dynamic interactions between unbound CHD with surface Si dimers and surface CHD adducts alter the picture provided by purely static methods. These kinetic effects, combined with two previously experimentally unidentified adducts, help reconcile the experimental with the thermodynamic product distribution. In the process, we emphasize the strengths and weaknesses of the various theoretical methods. Ultimately, we aim to glean principles that suggest ways to control the thermodynamics and kinetics of the reactions and enable the design of specific organic nanostructures on semiconducting surfaces.

2. Computational Details

AIMD calculations were performed using the Car−Parrinello technique[29] as implemented in the PINY_MD code.[32] Kohn−Sham orbitals were expanded in a plane-wave basis with a kinetic energy cutoff of 35 Ry. To reduce the computational expense, Troullier−Martins norm-conserving pseudopotentials in the Kleinman−Bylander separable form were used,[33] with S, P, and D treated as local for H, C, and Si, respectively, to calculate the ion−electron interaction. The Coulombic energy calculation utilized the two-dimensional reciprocal-space screening function approach[34] to properly account for the surface boundary conditions. Exchange was treated at the GGA level with the PBE functional,[35] while correlation was treated using the Perdew−Wang fit[36] to the uniform electron gas correlation data of Ceperley and Alder.[37] The bulk equilibrium lattice constant, as determined from Murnaghan's equation of state, is 5.470 Å. The Si(100)-2×1 system is comprised of 16 2×1 units each five layers deep, with the bottom layer fixed at the bulk lattice positions and terminated with H. The top surface forms two rows of four buckled dimers each. The larger surface dimensions prevent periodic images from interacting with themselves and eliminate the need for k-point sampling beyond the gamma point. For the reconstructed surface and reconstructed surface plus cyclohexadiene (CHD), the simulation box dimensions were $L_x = 15.47$ Å, $L_y = 15.5$ Å, and $L_z = 21.8$ Å, and $L_x = 15.47$ Å, $L_y = 15.5$ Å, and $L_z = 31.8$ Å, respectively, where the *z*-direction is the non-periodic direction.

First, the cyclohexadiene and reconstructed silicon surface were equilibrated separately using Nosé−Hoover chain thermostats[38] at 300 K for over 1 ps each to obtain realistic starting configurations. These calculations used a time step of 0.1 fs and fictitious CP masses of 670 and 990 au, respectively. The final time averaged configurations compared favorably with published experimental structures. All trajectories used the same initial configuration for the CHD and the Si surface but varied in the position and orientation of CHD. The CHD was placed 3 Å above the surface, as defined by the lowest point on the CHD and highest point on the surface. This is far enough away for the CHD to only be slightly perturbed by the presence of the surface, but still react with the surface when released. To maintain adiabaticity for longer periods of time in the combined CHD + Si system, the time step was dropped to 0.05 fs and the fictitious CP mass lowered to 400 au. First, the combined system was annealed from 0 to 300 K under NVE conditions. Next, the center of mass of the CHD was fixed while the system was equilibrated for 1 ps using Nosé−Hoover chains[38] under NVT conditions. Finally, the thermostat and center of mass constraint were removed and the dynamics were followed until an adduct formed or the trajectory became too long without formation of an adduct.

A second series of trajectories explored how surface coverage affects the reaction dynamics by adding a second CHD. The same procedure of annealing, equilibrating, and data gathering was followed as the single CHD case, except that the initial configuration was taken from a single CHD trajectory where the adduct had already formed. The second CHD was placed 3 Å above the surface away from the first CHD and was equilibrated with a fixed center of mass.

3. Results and Discussion

3.1. Unperturbed Si Dimer Structure and Dynamics. The Si(100)-2×1 surface consists of parallel rows of silicon dimers that are known to buckle at temperatures ranging from 10 K to room temperature.[39,40] The surface morphology has important ramifications for both the reactivity and the reaction mechanisms. In particular, a charge asymmetry is created due to the buckling, in which the "down" Si acquires a slight positive charge and the "up" Si acquires a slight negative charge. At 300 K, the buckling pattern is not static. Rather, the dimers can flip or "rock" about the unbuckled position. The role of the surface dynamics in the reaction mechanism with conjugated dienes has not yet been elucidated.

Both theoretical and experimental studies suggest that asymmetric surface dimer flipping at 300 K produces the characteristic (2×1) symmetric dimer pattern observed with STM. Experimental electron energy loss spectroscopy gives a dimer rocking frequency of 20 meV (∼200 fs) at 300 K,[41] but does not reveal how frequently the dimer flips to the opposite orientation. Classical[42,43] and quantum[44] molecular dynamics simulations confirm the rocking period is between 200 and 300 fs, while the flipping period ranges from 200 fs to more than 1.5 ps. The instantaneous dimer configuration determines which type of local environment, symmetric versus asymmetric Si dimers, a potential adduct will likely encounter. From the start of an NVE simulation to roughly 100 fs before a CHD−Si bond forms, the surface dimers exhibit a rocking period of ∼170 fs and spend only 5% of their time with a tilt angle of 5° or less. In most trajectories, only 2−3 out of the 8 dimers ever approach a zero tilt angle, let alone flip (i.e., at least 5° tilt angle in the opposite orientation). Of those that flip, the time the dimer resides in the opposite orientation varies widely, from as little as 100 fs to more than 5 ps. The limited statistics due to the similar starting configuration and short trajectory length (662 fs to 12.2 ps) allow only qualitative conclusions to be drawn. The two most important results for this study are that limited dimer flipping does occur on the time scale of the reaction and that the dimers are asymmetric the majority of the time.

(30) Minary, P.; Tuckerman, M. *J. Am. Chem. Soc.* **2004**, *126*, 13920.
(31) Minary, P.; Tuckerman, M. *J. Am. Chem. Soc.* **2005**, *127*, 1110.
(32) Tuckerman, M.; Yarne, D.; Samuelson, S.; Hughes, A.; Martyna, G. *Comput. Phys. Commun.* **2000**, *128*, 333−376.
(33) Kleinman, L.; Bylander, D. *Phys. Rev. Lett.* **1982**, *48*, 1425.
(34) Minary, P.; Tuckerman, M.; Pihakari, K.; Martyna, G. *J. Chem. Phys.* **2002**, *116*, 5351−5362.
(35) Perdew, J.; Burke, K.; Ernzerhof, M. *Phys. Rev. Lett.* **1996**, *77*, 3865−3868.
(36) Perdew, J.; Wang, Y. *Phys. Rev. B* **1992**, *45*, 13244.
(37) Ceperley, D.; Alder, B. *Phys. Rev. Lett.* **1980**, *45*, 566−569.
(38) Martyna, G. J.; Klein, M. L.; Tuckerman, M. *J. Chem. Phys.* **1992**, *97*, 2635−2643.
(39) Over, H.; Wasserfall, J.; Ranke, W.; Ambiatello, C.; Sawitzki, R.; Wolf, D.; Moritz, W. *Phys. Rev. B* **1997**, *55*, 4731−4736.
(40) Ono, M.; Kamoshida, A.; Matsuura, E.; Ishikawa, T. E.; Hasegawa, Y. *Phys. Rev. B* **2003**, *67*, 201306.
(41) Takagi, N.; Shimonaka, S.; Aruga, T.; Nishijima, M. *Phys. Rev. B* **1999**, *60*, 10919−10925.
(42) Weakliem, P.; Smith, G.; Carter, E. *Surf. Sci. Lett.* **1990**, *232*, L219−L223.
(43) Gryko, J.; Allen, R. *Ultramicroscopy* **1992**, *42−44*, 793−800.
(44) Stoll, E.; Baratoff, A.; Mangili, A.; Maric, D. *Mater. Sci. Eng.* **1996**, *B37*, 155−157.

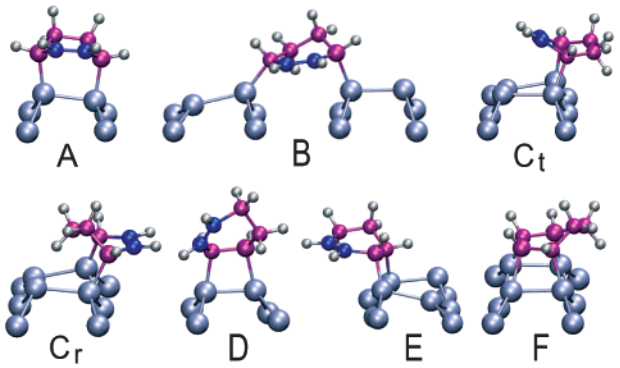

Figure 1. Snapshots of 1,3-CHD adducts that form on the Si(100)-2×1 surface at 300 K. Si, H, and C atoms are light blue, silver, and purple, respectively. The remaining C π-bond appears in dark blue. Only the Si dimer and atoms attached to the dimer are shown for clarity. Letters label the various adducts: (A) [4+2] intradimer (Diels−Alder type), (B) [4+2] interdimer across trough, (C_t) [4+2] interdimer same row with CH_2 above trough, (C_r) [4+2] interdimer same row with CH_2 above row, (D) [2+2] intradimer, (E) [2+2] interdimer, and (F) [4+4] 4-bond.

3.2. Observed Adducts. Figure 1 shows the adducts that form when 1,3-CHD reacts with the Si(100)-2×1 surface at 300 K. Atomic positions are taken directly from the trajectories. Thus, the relative positions vary with time, although the bonding connectivity remains conserved. We observe four (A, B, C_t, and D) out of the five STM-identified cycloaddition products[20] as well as four additional adducts. The most probable adduct, (C) [4+2] interdimer in the same row, which occurs in roughly 29% of the reactions, splits into two isomers that differ in the orientation of the CH_2 group. In the previously predicted case (C_t), the CH_2 groups are over the trough, while in the new case (C_r), the CH_2 groups are over the dimer row. Previous static DFT calculations found that C_r is slightly favored over C_t,[28,45] consistent with our results. We suggest that the experiment is unable to distinguish between the two isomers due to the symmetry of the adduct and strong unpaired Si−adduct orbital interactions. Likewise, the [2+2] interdimer adduct (E) is oriented such that the π-bond is over the trough, not the dimer row as identified in the STM experiment. However, this adduct may be able to flip orientation to match the experimentally derived structure because the barrier to move the H nearest the Si from the dimer to the trough side of the CHD should be small. In another case, both π-bonds in the CHD reacted to form a 4-bond adduct as predicted by Lee et al.[24] (labeled 5 in their notation), although the actual mechanism is somewhat different. Finally, an H-abstraction from a partially reacted CHD occurs during one trajectory. H-abstraction has been observed experimentally between 400 and 700 K.[22] Its presence in our simulation either indicates (1) H-abstraction does occur at lower temperatures, but in such small quantities that it is not detectable experimentally, (2) the extra energy released from the first bond formation created a local hot-spot, or (3) the barriers for H-abstraction are too low at this level of theory.

Because of the computational expense, only 15 trajectories were run: 11 with one CHD, 4 with two CHD. Figure 2 shows the starting position and center of mass of CHD for the 11 single CHD trajectories. CHD is sensitive to its relative orientation with respect to the dynamically changing surface dimers. Not only do different initial conditions at the same starting location produce different products, but the CHD often searches over several Si dimers (6 to >44 Å) before finding favorable reaction conditions. The final product distributions are given in Table 1, together with populations from STM measurements of Teague and Boland.[21] Thermodynamic considerations alone would predict a product distribution decreasing from A to E or from A to E with B and C switched at the multireference MP2[24] and DFT[28] level of theory, respectively. Adduct E is identified with the STM-derived adduct E because they share the same connectivity, although a different orientation relative to the dimer row. One trajectory did not react within 12.4 ps and hence is omitted from the statistics. Given the small number of trajectories and similar starting configurations, exact agreement with the experimental adduct distribution would be largely fortuitous. Nevertheless, Minary and Tuckerman[31] found that a larger ensemble of trajectories for 1,3-butadiene yielded a product distribution in close agreement with experiment. Hence, the reasonable agreement with experiment observed in Table 1 is not entirely unexpected. As in the experiment, we do find a high probability of forming (C) [4+2] interdimer adducts. A large contributing factor, discounted up to this point due to the assumption of either a concerted reaction mechanism or the existence of only the (C_t) adduct, is the availability of reactive sites. All products form via a two-step mechanism. Thus, once the first CHD−Si bond forms, (C) and (E) can react with Si on

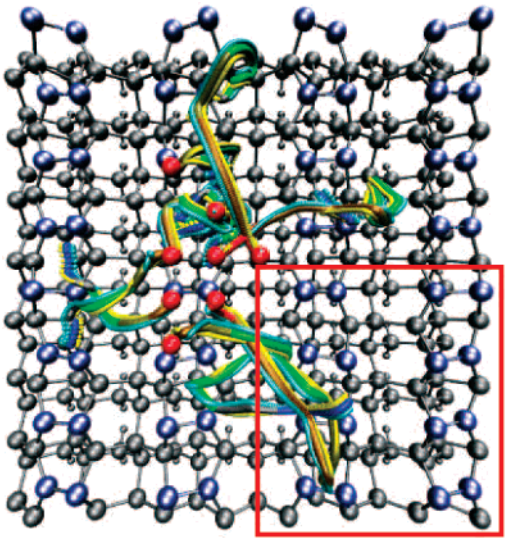

Figure 2. Summary of all single CHD trajectories. Red spheres mark the starting positions, and the red box delineates a single simulation cell. Si dimers, Si, and H are represented by large blue, large gray, and small gray spheres, respectively. The middle line denotes the center of mass of CHD from the beginning (red) to the end (blue) of the trajectory. Aqua and yellow lines represent the CH_2 and C=C sides of CHD, respectively. CHD often travels past several dimers, while rotating and occasionally being deflected by a dimer, before finding a favorable reaction environment.

Table 1. Final Product Distribution[a]

adduct	theory (%)	expt[b] (%)	adduct	theory (%)	expt[b] (%)
A	7.1	11 ± 3	D	28.6	10 ± 6
B	7.1	16 ± 7	E	7.1	12 ± 9
C_t	7.1	31 ± 6	other	21.4	21 ± 5
C_r	21.4	0			

[a] Based on 14 trajectories. Adducts (A−E) appear in Figure 1. "Other" includes the following products: one bond only, 4-bond product (adduct F in Table 1), and one bond plus H-abstraction. The trajectory that never reacted is omitted. [b] Reference 21.

(45) Note that Teague et al.[28] give conflicting C_t and C_r ordering in Table 1 versus Figure 2 and the text.

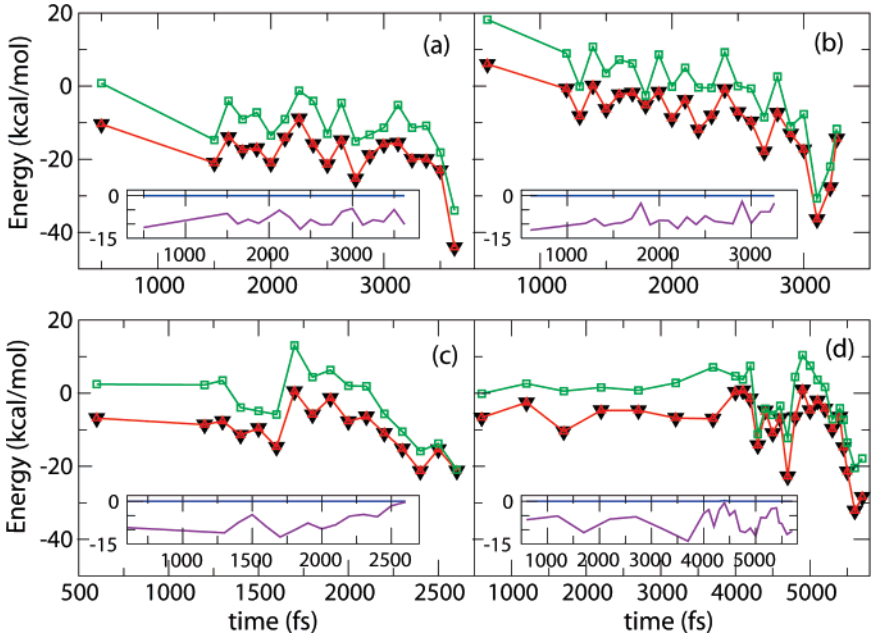

Figure 3. Comparison of SR (black ▼), singlet SU (red ▲), and triplet SU (green □) 0 K single point energies (kcal/mol) relative to the isolated CHD and Si(100) surface. Insets show the energy difference (kcal/mol) between SR−singlet SU (blue line) and SR−triplet SU (purple line). Representative configurations taken along 300 K trajectories for the (a) [4+2] intradimer [A], (b) [4+2] interdimer (same row) with CH_2 over the trough [C_t], (c) interdimer (same row) with CH_2 over the dimer row [C_r], and (d) 4 bond adducts [F]. A singlet radical mechanism is never favorable, although a triplet diradical mechanism may be possible during (b) and (d).

either adjacent Si dimer while the remaining adducts are restricted to one site only. In theory, (C_t) could form with either adjacent dimer, but in practice, the intermediate reacts with the first available site. At least within our trajectories, another reactive site will form a second bond before the tethered CHD has time to flip orientations, effectively limiting (C_t) to one site only. Although adduct (E) formation is enhanced by two possible reactive sites, the CHD ring restricts the number of paths that bring the second C close enough to react.

Within the "other" category is a fluxional species that could not be resolved via STM. Adduct isomerization of the [2+2] adducts has been proposed as one possible cause of the fluxional species.[21] At least on the 1.4 ps time scale, we see no evidence of this isomerization, although we cannot exclude longer-time events. STM-induced rearrangements likely play a major role. Both styrene and cyclopentene on Si(100) rearrange under large bias conditions.[5] In an attempt to explore whether molecular charging, which might occur during the STM measurements, stabilizes a partially reacted cyclohexadiene, we added an extra electron to a system after a CHD had formed just one bond with the surface. The CHD intermediate forms an adduct within 400 fs, indicating that simply charging the system is not sufficient. The electron localization function (ELF)[46] reveals that the extra electron is not localized on the CHD, at least under the local spin density approximation. Steric hindrance due to a nearby CHD may contribute. In one trajectory, a second CHD remains trapped in an intermediate state for at least 4 ps due to constraints imposed by a CHD already attached to a dimer one row over and two dimers down. Although not long by experimental measures, it hints that long-range interactions and surface crowding may stabilize intermediate species.

Both Tersoff−Hamann[47] and Bardeen Perturbation Theory[48] STM images were generated for our adduct structures. Despite a similar appearance between the computed and measured images, we could not reconcile the computed images with the traditional interpretation of the experimental STM images, that the C=C π^* orbitals characterize the CHD adduct. Rather, the CH_2 groups dominate the computed images. The failure arises from a poor description of the virtual orbitals in the vacuum region and a breakdown of the assumption that tip and adduct orbitals do not interact. Results suggest that low-lying unoccupied orbitals change shape due to finite temperature fluctuations of the adduct atomic positions, even though the adduct connectivity remains unchanged. This variability has two consequences: (1) theoretically derived STM images should be time-averaged over finite temperature configurations; (2) and STM tip-induced conformation changes may contribute to the apparent negative differential resistance seen in similar systems as suggested by Pitters and Wolkow.[5] The limitations of these standard theoretical techniques, when applied to high-resolution empty-state imaging of conjugated systems attached to Si dimerized surfaces, will be explored in-depth in a future paper.

3.3. Radical Mechanism? Lee et al.'s[24] cluster-based multireference second-order perturbation theory study of the minimum energy pathways for the cycloaddition of CHD to the Si(100)-2×1 surface suggested that diradical mechanisms should play a major role. Theoretical calculations are at an impasse. Despite experimental evidence to the contrary,[39,49] multireference cluster calculations predict that Si surface dimers are symmetric,[50] not tilted, which could alter reaction pathways. The periodic DFT calculations performed here capture the correct dimer tilt. At the same time, these calculations neglect surface crossing events because they are single reference.

(46) Savin, A.; Jepsen, O.; Flad, J.; Andersen, O.; Preuss, H.; von Schnering, H. *Angew. Chem.* **1992**, *31*, 187−188.
(47) Tersoff, J.; Hamann, D. *Phys. Rev. B* **1985**, *31*, 805−813.
(48) Bardeen, J. *Phys. Rev. Lett.* **1961**, *6*, 57−59.
(49) Mizuno, S.; Shirasawa, T.; Shiraishi, Y.; Tochihara, H. *J. Chem. Phys.* **2006**, *124*, 081105.
(50) Olson, R.; Gordon, M. *J. Chem. Phys.* **2006**, *124*, 081105.

Table 2. Time (fs) between First and Second Bond Formation[a]

adduct	time	adduct	time	adduct	time	adduct	time
A	1891	C_t	833	D	438/479/1555/474	1-bond	>4127
B	259	C_r	135/378/1298	E	1000	4-bond	1233

[a] Time in femtoseconds. Adducts (A−E) appear in Figure 1. The "/" separates different trajectories. The 3rd and 4th bonds appear in the 4-bond adduct after 2 and 126 fs, respectively.

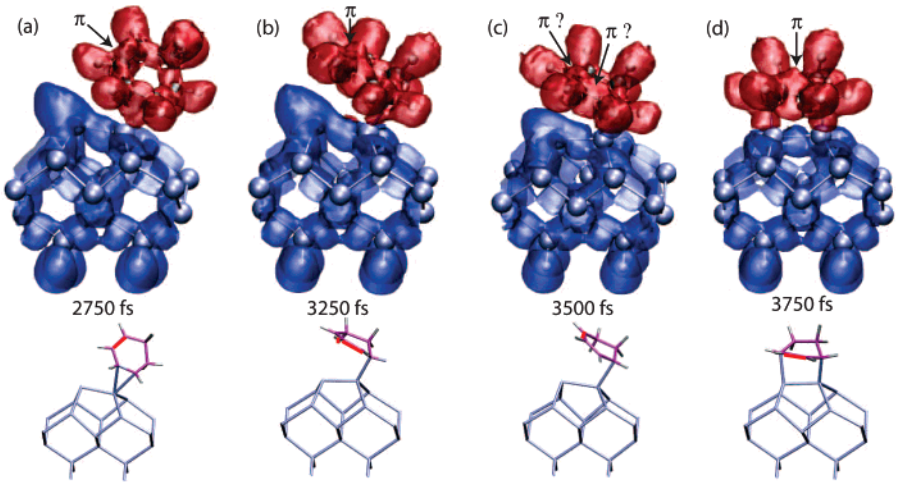

Figure 4. Two-step reaction mechanism for the [4+2] intradimer [A] adduct. The ELF is approximately divided between contributions due to CHD (red) and the Si surface (blue). Stick figures at the bottom show all bonds, with the π-bonds highlighted in red. The first bond shifts between a "down" Si and (a) the middle of a π-bond or (b) the C closest to the CH_2 groups. In (c), the π-bond delocalizes between three adjacent C's. Finally, in (d), the negative "up" Si reacts with the positive C next to the CH_2 groups to form the adduct.

To estimate how important radical mechanisms and surface crossings might be during adduct formation, we calculate single point energies along four representative trajectories for three spin states: spin-restricted (SR), which assumes that all electrons are paired (singlet), spin-unrestricted (SU) with the same number of up and down electrons (singlet), and SU with two more up than down electrons (triplet). The SU calculations mimic diradical electronic configurations by allowing up and down electrons to vary spatially to lower the energy. If the up and down electron densities are identical, the SU singlet functional simply reduces to SR. Because DFT is a variational theory, the lowest energy configuration is thermodynamically favorable. Therefore, if the electronic configuration of the lowest energy state changes, a surface crossing might occur even though it is not allowed within standard DFT.

Figure 3 compares the three energies for four representative trajectories. Single point energy calculations were carried out at 0 K using configurations taken from the 300 K trajectory. In all cases, the SR (black ▼) and SU singlet (red ▲) single point energies were essentially identical (the blue line is the energy difference), revealing that spin polarization is not necessary for the singlet case. The SU triplet (green □) energies are always higher in energy than the SR energies (purple line is the energy difference), although sometimes the difference is within the error of the calculation as seen in (b) the [4+2] interdimer adduct (C_t) and (d) the 4-bond adduct. At no point in (a), the [4+2] intradimer adduct, does the triplet state become likely. In (c), the previously unpredicted [4+2] interdimer adduct (C_r), only the final adduct, not the transition state, exhibits comparable singlet and triplet energies. Since we are most interested in reaction mechanisms during the adduct formation, the triplet influence should be negligible. We also verified that SR is sufficiently accurate for our system by rerunning a trajectory that formed the (C_r) [4+2] interdimer adduct shown in Figure 3c using singlet SU. Although there were some variations, the same final adduct formed. Because of the difference between DFT periodic and multireference cluster systems, a definitive statement on the reaction mechanism cannot be made. Our work reveals that within periodic plane-wave GGA DFT the spin-restricted reaction mechanisms studied are favored over the equivalent triplet mechanisms and hence should play the major role.

3.4. Reaction Mechanism. In all cases, the reaction mechanism involves two distinct steps separated by an intermediate that persists from 135 fs to over 4 ps. Table 2 lists the lifetime of the one C−Si bond intermediate, where a bond is assumed to have formed when the C−Si distance first reaches 2.4 Å. The ELF reveals that this is a conservative estimate of bond formation. Figure 4 shows that the reaction mechanism to form the [4+2] intradimer adduct [A] is consistent with the closely related 1,3-butadiene + Si(100)-2×1 system.[30,31] First, a positively charged "down" Si reacts with one of the negatively charged carbon π-bonds. The first bond, as revealed by the ELF, can shift between the two carbons. The remaining π-bond, which appears as a slight protrusion in the ELF, eventually delocalizes over the three C's [C═C−C^+ ↔ $^+$C−C═C] before the positively charged carbon reacts with the "up" Si to form the [2+4] intradimer adduct.

How much do geometry and relative orientation dictate the product distribution? Qualitatively, a first bond will form if a π-bond comes within ~3.0 Å of a "down" Si without any other atom interfering, and a second bond forms if a resonant-C (i.e., a C^+ in the extended π-system) comes within ~3.0 Å of any Si. Within the limited statistics, Figures 5 and 6 analyze which structural properties are important. A labeled CHD appears in the inset of Figure 5a. In the following, d_{C-Si} is the C_n (n =

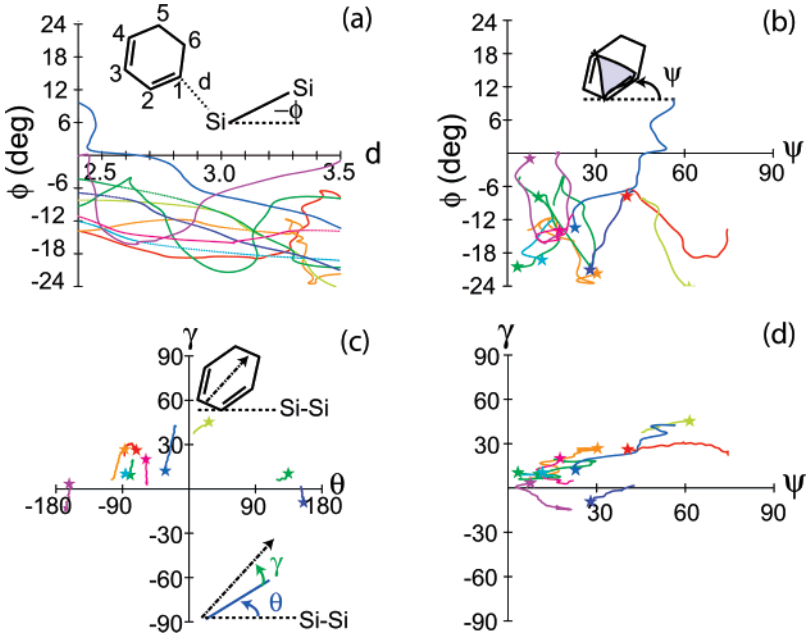

Figure 5. Properties in the reactive region immediately prior to the first bond formation. The colors denote different trajectories. d_{C-Si} is the distance between the C and Si in the first bond. Stars appear at $d_{C-Si} = 3.5$ Å. (a) d_{C-Si} versus the dimer tilt angle (ϕ). All of the dimers are oriented down relative to CHD. (b) Angle between the plane defined by π-bonds with the $z = 0$ plane (ψ) versus the dimer tilt angle for all d_{C-Si}. The dimer tilt changes more rapidly than the CHD tilt. (c) $\mathbf{R}_{bisec}$ is the vector connecting the midpoints of C_1-C_2 and C_5-C_6. Angle between R_{bisec} projected onto the surface and the closest Si dimer (θ) versus angle between $\mathbf{R}_{bisec}$ and the $z = 0$ plane (γ) for all d_{C-Si}. CHD is horizontal only when the CH_2 groups are oriented away from the Si dimer. (d) ψ versus γ for all d_{C-Si}. At small angles, the orientation with the surface is nearly identical. At larger ψ, γ changes more slowly, indicating that the C=C bonds tilt relative to the surface more than the $\mathbf{R}_{bisec}$ axis.

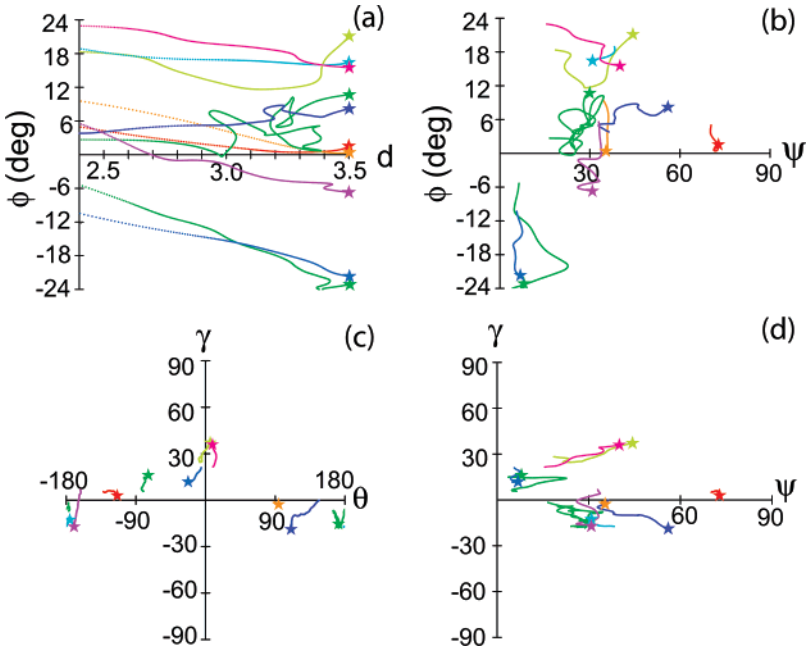

Figure 6. Properties in the reactive region immediately prior to the second bond formation. All variables are defined as in Figure 5. (a) The Si in the second bond is usually on the "up" end of the dimer. (b) The Si dimer tilts more rapidly than the CHD. There may be a preferred CHD tilt at ~30°. (c) The bulky CH_2 groups either point up ~90° or ~180° relative to the reactive Si dimer. (d) When CH_2 groups point up, $\mathbf{R}_{bisec}$ and the CHD π-systems often tilt simultaneously. Otherwise, the CHD tends to rotate around $\mathbf{R}_{bisec}$.

1,4)−Si distance for the first bond that forms. Figure 5a plots d_{C-Si} versus Si dimer tilt angles in the initial reactive region, 3.5−2.4 Å. All of the dimer tilt angles are negative, showing that "down" Si are more reactive. Figure 5b attempts to quantify whether the tilt of CHD matters by measuring the angle between the surface and a plane defined by $C_1-C_2-C_4$ versus the Si dimer tilt angle for all reactive d_{C-Si}. Although CHD has a slight preference to approach the Si dimer relatively horizontally ($\psi < 30°$), there is no apparent correlation with dimer tilt angle. Figure 5c measures the relative orientation of the bulky CH_2 groups relative to the closest Si dimer by plotting the angle θ formed between the vector $\mathbf{R}_{bisec}$ connecting the midpoints of C_2-C_3 and C_5-C_6 and the closest Si dimer versus the angle γ formed between R_{bisec} and the $z = 0$ plane for all reactive d_{C-Si}. As expected, the CH_2 groups always point up ($\gamma \approx 30°$) when they are oriented toward the Si dimers ($|\theta| < 40°$) or horizontal

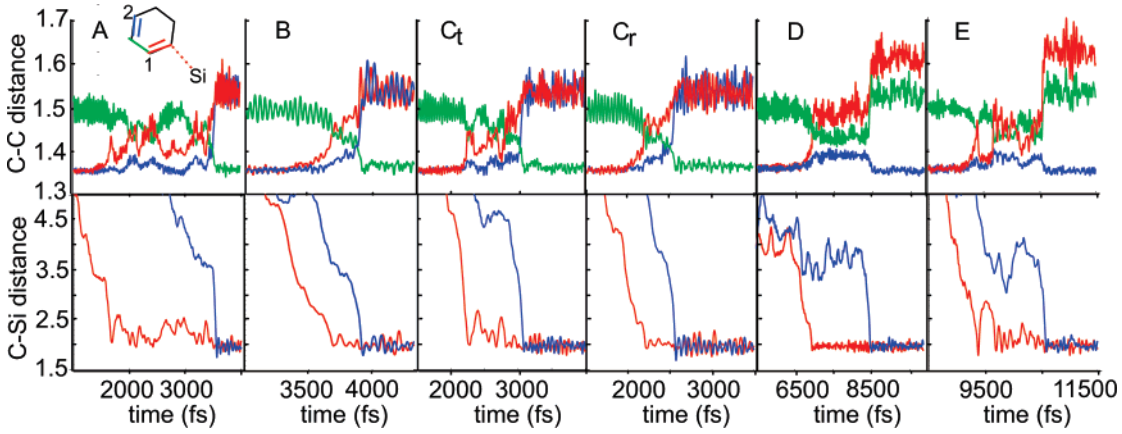

Figure 7. The top row shows the three possible π-bond lengths averaged over 25 fs for the adducts (see Figure 1) in the reactive region. The bottom row displays the corresponding first and second C−Si bond lengths in red and blue, respectively. The small figure in (A) labels the three C−C bonds and the first C−Si bond. The second C−Si would form at positions 1 or 2. All distances are given in angstroms. During the reaction, the C−C and C═C bond lengths fluctuate significantly. After the adduct forms, the remaining π-bond reverts to the original length, while the single C−C bonds are expanded. Change in the π-bond lengths coincides with C−Si bond formation.

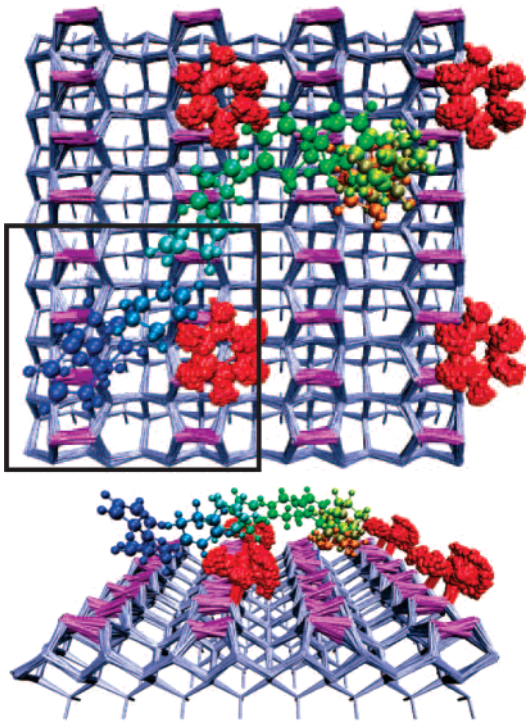

Figure 8. Top and side view of snapshots taken at 1 ps and 100 fs intervals for the free CHD and the rest of the system, respectively, during a 11.5 ps two-CHD trajectory. The first CHD forms C_t (Figure 1, top right). The second CHD forms E [see Figure 1] after 10.5 ps. Si, H, Si dimers, and the first CHD are shown in light blue, silver, purple, and red, respectively. Snapshots of the second CHD start in blue at $t = 0$ ps and gradually change to orange at $t = 11$ ps. Four unit cells (black box) are shown. The distance between the center of mass of both CHD always remains greater than 5.55 Å, effectively protecting adjacent Si dimers.

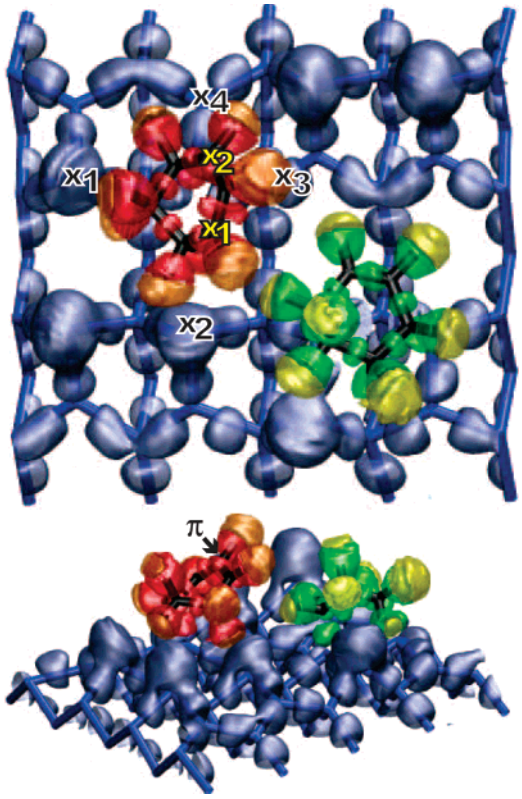

Figure 9. ELF of a [4+2] interdimer adduct (green/yellow) and a partially reacted CHD (red/orange) on Si. Potential reactive Si and C sites are marked with black X's and yellow x's, respectively. π shows the location of the remaining double bond. Only the top three Si layers are shown for clarity. The red and green areas map the area within a 2.775 Å radius of the CHD center of mass. The adduct distorts nearby Si "up" lobes, demonstrating that adducts can protect nearby reactive Si sites. The local dimer tilt configuration and the CHD adduct delay the formation of the second C−Si bond.

($\gamma \approx 0°$) when they are oriented away ($\theta = \pm 180°$). Figure 5d looks at how CHD prefers to tilt by plotting ψ versus γ for all reactive d_{C-Si}. At small tilt angles, both ψ and γ change by equivalent amounts, while at larger ψ, γ changes more slowly, indicating a slight preference to tilt around $\mathbf{R}_{bisec}$. This is consistent with either C_1 or C_4 tilting toward the surface to form a C−Si bond. Figure 6 shows the same orientation information for the second C−Si bond. As expected, in (a) the second bond generally forms between an "up" Si and resonant C. In the two exceptions, the π-system approaches the Si dimer nearly horizontally, resulting in [B] and [C_r] adducts. The other trends are the same as for the first C−Si bond, if slightly more pronounced due to the constraint of the first bond. In particular, there seems to be a favored CH_2 orientation (Figure 6c) at $\theta = \pm 90°$, where θ is the angle between the projection of $\mathbf{R}_{bisec}$ onto the x-y plane and the closest Si dimer.

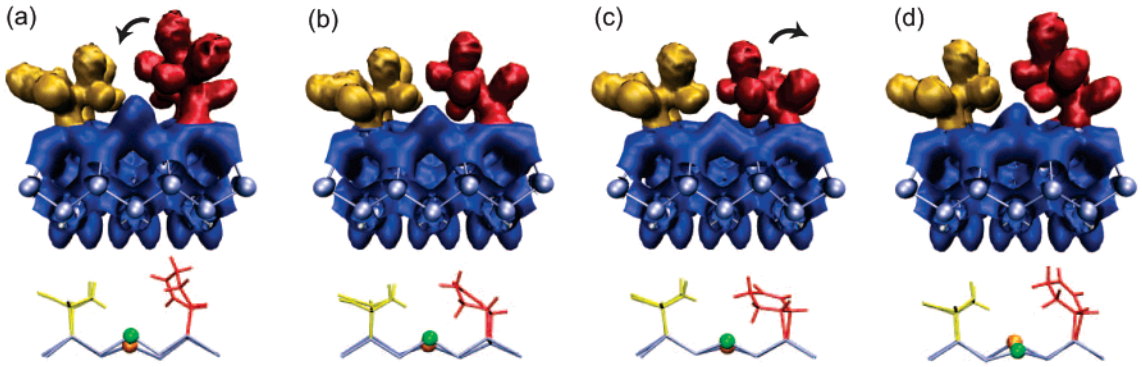

Figure 10. Side view of Si dimer row. Si atoms are shown as spheres. ELF function associated with [4+2] (yellow) and [2+2] (red) intradimer CHD adducts, and Si (blue) reveals that adduct dynamics can induce dimer flipping. Stick figures of the atomic positions appear at the bottom. The green (front) and orange (back) spheres highlight the dimer that flips. (a) Initially, the dimer between the two adducts is "up" closest to viewer. (b) As the [2+2] interdimer adduct moves toward the left, the CH_2 groups push on the "up" Si, causing the ELF to decrease. (c) At the smallest [2+2] interdimer adduct−Si dimer separation, the dimer remains tilted toward the viewer. (d) The dimer finally flips after the adduct starts to return to the upright position. The total time to flip a dimer is less than 300 fs.

Figure 7 plots (top row) the three C−C distances in the conjugated region [$|C_1-C_2|$, $|C_2-C_3|$, and $|C_3-C_4|$ averaged over 25 fs] and (bottom row) the first (red) and second (blue) C−Si bonds versus time in the reactive region for representative trajectories of each adduct given in Figure 4. Before the first C−Si bond forms, there are clearly two π-bonds; after the second C−Si bond forms, only one π-bond remains. The intermediate regime starts when one of the C−C π-bonds lengthens and a C−Si bond rapidly forms and ends when two single C−C bonds and a second C−Si bond form. In the intermediate region, the C−C bond order is less clear based on bond length alone. What is unambiguous is a two-step mechanism characterized by an intermediate, which persists for at least 250 fs (B). In the first four [4+2] adducts (from left), the second bond forms when the π-bond switches position (blue to green), while in the last two [2+2] adducts, the original π-bond becomes a strained single C−C bond.

The 300 K molecular dynamics trajectories reveal several trends not readily apparent in 0 K static calculations. Static calculations predict both symmetric dimer and asymmetric dimer reaction mechanisms, while the molecular dynamics simulations proceed solely by the two-step asymmetric carbocation mechanism. The relatively long-lived intermediate allows the second Si−C bond to form at any available site, sometimes resulting in a different adduct than the initial CHD position might imply. Furthermore, the dynamics show that the dimer flipping enhances adduct formation when properly oriented as detailed above, but redirects the CHD when it is not, producing a nonuniform search of the surface. The resulting directed surface exploration may favor certain adducts, but significantly more trajectories would be necessary to verify this effect.

3.5. Higher CHD Coverage. The presence of a CHD adduct on the surface alters how a second CHD explores the surface and ultimately reacts. Four different surface adducts were chosen: [4+2] intradimer, [4+2] interdimer with the CH_2 over the trough, [4+2] interdimer with the CH_2 over the row, and [2+2] intradimer. The dominant effect in all cases is one of steric hindrance. Figure 8 shows the trajectory of a CHD on the Si surface with a [4+2] interdimer adduct [C_r] already attached taken at 1 ps intervals. Several features are immediately apparent. First, like the single CHD case, the surface dimers flip on the time frame of the reaction, allowing dynamic surface effects to influence the adduct formation. Second, the surface adduct (red) redirects the free CHD (blue at $t = 0$ gradually changes to orange) whenever it approaches too closely. In all of the two-CHD trajectories, the centers of mass of the two CHDs are never less than 5.55 Å apart, and individual atoms remain at least 1.90 Å apart. For comparison, dimers are about 3.9 Å apart in a row and 5.5 Å apart across rows. The surface adduct has the effect of protecting nearby dimers from reacting with the CHD. The large effective size of each surface adduct also indicates the need for large simulation cells to avoid spurious constraints in the intermediate coverage regime.

Less obvious, but also important, are the attractive and repulsive forces exerted by the surface adducts on the free CHD. Typically, the CHD accelerates toward a nearby surface adduct, only to be repelled in a different direction when the CHD "encroaches" on the adduct's space. A similar spike in the center of mass velocity occurs whenever adduct formation conditions are favorable, like when the C═C π-bond of a free CHD points in the direction of a "down" Si. The main difference is the event frequency: surface adducts are easier to find than favorable Si dimer sites because the former protrude more from the surface.

Constraints imposed by surface adducts can have interesting physical consequences. Figure 9 shows the electron localization function (ELF) between a [4+2] interdimer adduct with the CH_2 groups over the dimer row (green/yellow) and a partially reacted CHD (red/orange). Note how the lobes on all of the "up" Si near either CHD are distorted, showing that influence of the bound CHD can extend across the trough. The black X's and yellow x's mark all potentially active Si and resonant C positions, respectively. None are in the correct local environment to form a C−Si bond. The red and green ELF highlight the region within a 2.775 Å radius of the CHD center of mass. While not touching, the borders remain close to each other and the relative CHD orientation nearly fixed for over 4 ps, hinting that either favorable interactions or steric hindrance are trapping the CHD in the vicinity of the adduct. The increased intermediate stability may contribute to the fluxional species STM signal. These adduct−unbound CHD interactions may also enhance local ordering by favoring adducts that are near, but outside the excluded zone. This ordering effect is expected to be much weaker than hydrogen passivation of the surface, as in styrene

wire formation on H-terminated Si(100),[19] which requires the extraction of an adjacent H for the reaction to proceed.

Surface adducts can also force dimers to flip. Figure 10 shows the ELF at 4 times during a trajectory with [4+2] (yellow) and [2+2] (red) interdimer adducts. The dimer between the two adducts flips to minimize the interaction between the Si dimer and the CH_2 groups (2.09 Å minimum distance). The short delay between the minimum Si−CH_2 distance and the dimer flip hints that CHD motion promotes the reaction. The extrema of the "bowing" motion of the [2+2] adduct ((a) versus (c)) corresponds to the two confomers predicted by Choi and Gordon.[25] We suspect that even one surface adduct can induce adjacent dimers to flip. Indeed, we see increased dimer flipping once an adduct forms. However, with only 15 trajectories, it is difficult to quantitatively conclude that the dimer flipping is due solely to the adduct, and not just the random flipping that normally occurs. The analysis problem is further exacerbated by the local hot spots caused by adduct formation. Although initially physical, the small system size prevents the temperature from re-equilibrating to 300 K as would occur experimentally.

4. Conclusion

Room-temperature AIMD simulations of the cycloaddition of CHD to the Si(100)-2×1 surface confirm the identity of four of the five STM-proposed surface adducts and suggest four additional products. All observed adducts form via a two-step carbocation mechanism. The majority of the discrepancy between the experimental and the thermodynamically predicted product distribution can be accounted for by two equivalent reaction sites for the [4+2] interdimer, same row adduct [C]. Radical mechanisms may play a role for certain adducts, but spin-unrestricted calculations confirm that single reference carbocation mechanisms should accurately describe many adduct formation pathways.

The local configuration strongly influences which adduct forms. The CHD can traverse more than 40 Å or 10 ps before finding favorable conditions. Conversely, the surface is "eager to please". For the first bond formation, if the C═C orbital is pointed toward a "down" Si without the CH_2 groups interfering with any neighboring dimers, the adduct and Si accelerate toward each other. The movement of surface dimers to form the second bond is even more dramatic. In certain instances, the reactive dimer can even flip orientation to allow an "up" Si to react with the CHD. Static calculations would miss the enhancement caused by dynamic dimer flipping.

Partial adduct coverage alters adduct formation in two fundamental ways. First, the physical presence effectively excludes a hemisphere of radius 5.55 Å, thereby protecting nearby Si dimers. This steric hindrance may contribute to the fluxional species observed in the STM image. Second, the surface adducts act as both attractors and repellers, ultimately causing free CHD to accelerate toward and away from surface adducts in a pinball type fashion.

The large number of available CHD surface adducts on Si precludes well-ordered nanostructures at higher coverage. The future design of organic−inorganic interfaces could take advantage of several mechanistic features to increase the uniformity of the final adducts. Many group IV materials like Ge and SiC form reactive surface dimers, but with different dimer spacing. If the dimers are sufficiently far apart, intradimer adducts should dominate. Steric hindrance caused by larger side groups may force the organic molecule to react in a specific orientation, thus favoring the adduct with the easiest access. Secondary interactions, such as those caused by H-bonding or π-stacking, may favor ordered structures at higher coverage by helping to orient the incoming organic molecules.

Acknowledgment. We acknowledge support from NSF CHE-0310107 and NSF CHE-0121375. We would also like to thank Dr. Anatole von Lilienfeld for useful discussions. All calculations were performed on a DEC 750 node Compact Alpha Server at the Pittsburgh Supercomputing Center, an SGI Altix 3700 Bx2 system obtained via NSF CHE-0420870, and an IBM eServer BladeCenter system with 256 JS20 nodes provided by NYU's ITS division.

Supporting Information Available: Part S0 contains a short description of the supplementary files. Movies of 1,3-CHD reacting with Si(100) to form adducts A−E shown in Figure 1 appear in parts S1−S6. Movies corresponding to Figure 9 and Figure 10 are given in parts S7 and S8, respectively. This material is available free of charge via the Internet at http://pubs.acs.org.

JA0724994